Biophysical Reports

ARTICLE

Correlating single-molecule rupture mechanics with cell population adhesion by yeast display

Mariana Sá Santos,[1,2,3] Haipei Liu,[1,2] Valentin Schittny,[1,2] Rosario Vanella,[1,2] and Michael A. Nash[1,2,*]

[1]Institute for Physical Chemistry, Department of Chemistry, University of Basel, Basel, Switzerland; [2]Department of Biosystems Science and Engineering, ETH Zurich, Basel, Switzerland; and [3]Systems Biology PhD program, Life Science Zurich Graduate School, Zurich, Switzerland

ABSTRACT Here, we present a method based on yeast surface display that allows for direct comparison between population-level cell adhesion strength and single-molecule receptor-ligand rupture mechanics. We developed a high-throughput yeast adhesion assay in which yeasts displaying monomeric streptavidin (mSA) or enhanced mutant mSA were adhered to a biotinylated coverglass submerged in fluid. After exposure to shear stress (20–1000 dyn/cm^2) by rapid spinning of the coverglass, cells were imaged to quantify the midpoint detachment shear stress for the cell population. We then performed atomic force microscope single-molecule force spectroscopy (SMFS) on purified mSA variants and identified correlations between single-molecule rupture force distributions and cell population adhesion strength. Several features of yeast display were important for successful correlations of adhesion strength to be drawn, including covalent attachment of the receptor to the cell wall, a precisely defined molecular pulling geometry, repression of nonspecific adhesion, and control for multivalency. With these factors properly taken into account, we show that spinning disk cell adhesion assays can be correlated with SMFS and are capable of screening the mechanical strength of receptor-ligand complexes. These workflow enhancements will accelerate research on mechanostable receptor-ligand complexes and receptor-mediated cell adhesion.

WHY IT MATTERS Cell adhesion is the process by which cells attach to various substrates, extracellular matrix components, and tissues through specific binding of protein receptors on the cell surface. This process is of widespread interest in biophysics and cell biology. Although cell adhesion is governed at the most basic level by the mechanical stability of receptor-ligand interactions, the development of unified biophysical assays that can correlate these properties when measured at different length scales (i.e., single-molecule versus cell population) is challenging. We address this issue by developing methodology to investigate correlations between adhesive phenotypes of cell populations and the mechanical strength of single-molecule receptor-ligand interactions.

INTRODUCTION

Understanding the mechanical properties of receptor-ligand complexes is fundamentally important in characterizing the biophysical behavior of native and engineered molecular systems. The classical paradigm of molecular recognition and binding affinity focuses exclusively on kinetic parameters at equilibrium. However, there are many scenarios in which proteins experience tension, compression, shear stress or mechanical force, and in these situations, the nonequilibrium mechanical stability of protein-protein interactions is of high interest. The fields of molecular biomechanics and force spectroscopy concern themselves with the biological significance of protein deformation under force, and its practical significance in areas such as cell adhesion, biomaterials science, therapeutics, and drug delivery.

Single-molecule force spectroscopy (SMFS) (1–4) with the atomic force microscope (AFM) is a valuable tool for characterizing protein nanomechanics (Fig. 1, *left*). Recent methodological developments now allow researchers to apply well-defined force protocols to polyprotein systems while taking into account aspects such as molecular pulling geometry (5–7), validation of single-molecule interactions using internal unfolding fingerprints (1,2), and generation of large statistics using reversible mechanostable pulling handles (8). Although these features allow AFM-based SMFS to provide quantitative descriptions of protein folding and

Submitted September 13, 2021, and accepted for publication November 22, 2021.

*Correspondence: michael.nash@unibas.ch

Editor: Aleksandra Radenovic.

https://doi.org/10.1016/j.bpr.2021.100035

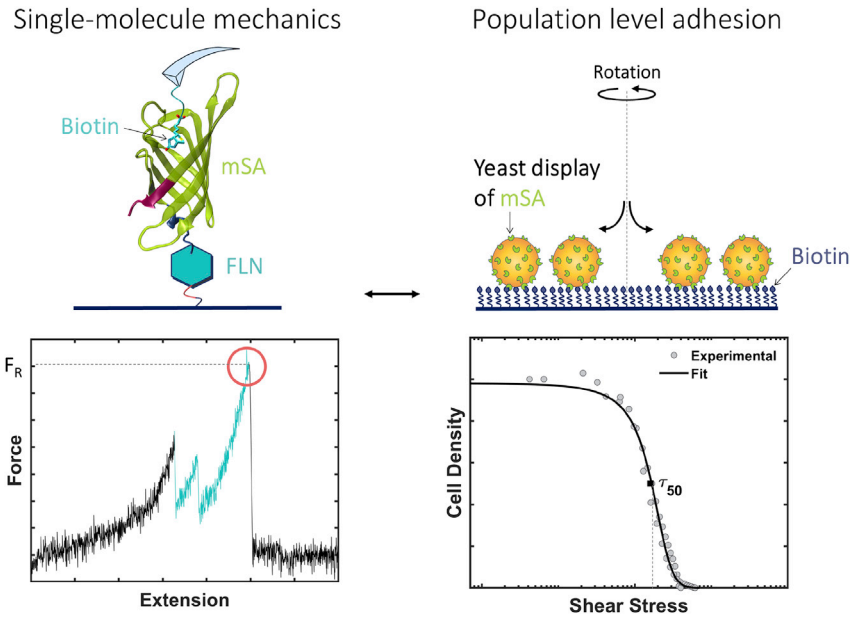

FIGURE 1 Conceptual schematic of correlating single-molecule rupture mechanics with population-level cell adhesion. (*Left*) A fusion protein comprising mSA fused to an FLN fingerprint domain is site-specifically attached to a coverglass. Probing the surface with a biotin-modified cantilever results in force versus extension traces, from which rupture forces (F_R) of individual biotin-mSA complexes are extracted. (*Right*) Yeast cells displaying mSA are adhered to a coverglass covalently modified with biotin. Spinning the coverglass in fluid generates a shear gradient at the surface that detaches cells. Plotting the cell density versus shear stress allows characterization of the midpoint shear stress required to detach half the cell population (τ_{50}). This study seeks to quantitatively correlate F_R with τ_{50} for mSA variants. The crystal structure of monomeric streptavidin-biotin complex (Protein Data Bank: 4JNJ (12)) was rendered with VMD - Visual Molecular Dynamics (13).

unfolding and unbinding energy landscapes, the technique requires sophisticated equipment and a high level of expertise. Production and purification of polyproteins in recombinant hosts, data collection, and analysis times are all lengthy, and AFM measurement throughput is low. Although in vitro transcription and translation systems combined with microfluidic technology (9) have been deployed to address this, the intrinsic serial nature of scanning probe methodology remains severely limiting.

Conversely, measurement systems for cell adhesive forces (10) typically do not require protein purification and benefit from shorter experimental run times and higher throughput. This throughput, however, comes at a cost of reduced resolution. In bulk cell adhesion assays, fast dynamics are not captured, pulling geometries and forces may be ill defined, and multivalency of interactions needs to be considered. The importance of accounting for multivalency is well understood in equilibrium-based selections of libraries using yeast surface display (11). In this case, immunostaining of the displayed proteins is used to normalize binding levels to expression levels (i.e., level of multivalency). To correlate mechanical behavior across length scales, a similar account must be taken for the level of multivalency of cell-surface interactions. This presents a challenge in directly correlating single-molecule mechanical stability of receptor-ligand bonds and bulk adhesion strength of a cell population.

For an appropriately designed system, however, both receptor-ligand AFM-SMFS and quantitative assays for cell adhesion strength should be governed by the same fundamentals, namely the mechanical strength of the adhesive complexes. Although many studies use either cell adhesion assays or single-molecule mechanical assays independently to quantify the mechanical stability of protein-protein interactions, very few (14–16) have considered correlations between cell adhesion under flow and single-molecule mechanics of the interactions that mediate adhesion. In this study, we aimed to explore these correlations and develop a system that could correlate cell population adhesion with single-molecule rupture events (Fig. 1).

We chose the hydrodynamic shear-based spinning disk assay (SDA) to quantify cell adhesion strength (Fig. 1, *right*). This assay has been extensively characterized and widely used in the past to quantify adhesion of mammalian cells on biomaterial surfaces (17–21). In comparison with other shear-based assays, SDAs produce high maximal shear stresses ($>$2500 dyn/cm^2) and do not require cumbersome microfabrication or precise flow rate control with pumps. Furthermore, SDAs expose cells in the population to a gradient of shear stress that grows linearly with distance from the center of the disk while maintaining uniform chemical conditions at the surface. As the disk spins, fluid flow over the surface mechanically strains the interactions between the proteins at the surface of the cells and immobilized surface ligands. Toward the outside of the disk the applied shear stress is significantly higher, and fewer cells can withstand the forces. The result is a sigmoidal decline in the number of adherent cells with respect to the shear stress. If the protein interaction is more resistant to mechanical force, a higher fraction of cells will remain further out from the center of the disk after spinning. The adhesion strength is then defined as the shear stress required to detach 50% of the cell population.

Yeast surface display is achieved by genetically fusing receptor genes to the Aga2p mating factor in *Saccharomyces cerevisiae* (22–24). This display system is widely used for selection of antibody libraries (25–28) and presents several advantageous features for comparative cell adhesion studies. The outer peptidoglycan cell wall of *S. cerevisiae* is mechanically rigid, meaning that the cells will minimally deform in response to moderate forces. The nearly spherical shape of yeast cells facilitates uniform application of force (29) by the flow field in the SDA. Prior studies have combined Aga2p-based yeast display with microchannel rolling adhesion assays on yeast cells under flow (29–31); however, to the best of our knowledge, yeasts have not been used in the SDA.

As a model receptor for our study, we chose monomeric streptavidin (mSA) and its previously reported (32) mutant mSA(S25H). Biotin-streptavidin technology has been extensively used in immunodetection and labeling systems (33); however, the tetrameric structure of streptavidin with four biotin binding sites can lead to unwanted clustering of biotinylated ligands. To address this, several groups generated monomeric versions of streptavidin using rational approaches (34–36). Park and colleagues engineered a monomeric streptavidin (37) by inserting binding site loops derived from a dimeric streptavidin homolog, rhizavidin, into a streptavidin monomer. A serine to histidine mutation at position 25 was used to generate the mutant mSA(S25H) with a significantly decreased kinetic off rate (12) and $K_D = \sim 1$ nM. Here, we fused mSA and its variant S25H to the Aga2p display anchor protein of *S. cerevisiae*. We then displayed artificial mSA receptors on the yeast surface as well as producing them as soluble proteins in *Escherichia coli*. By comparing the mechanostability of the mSA-biotin interaction using both AFM-SMFS and SDA, we sought to harmonize the observations on a validated set of receptors with known affinity and mechanics.

MATERIALS AND METHODS

Materials

All chemicals used in this study were purchased from Sigma-Aldrich (St. Louis, MO) unless otherwise stated. Primary and secondary antibodies were obtained from Thermo Fisher Scientific (Waltham, MA). Biotin-Atto565 was acquired from ATTO-TEC GmbH (Siegen, Germany). Polymerase chain reaction (PCR) buffers and enzymes were from New England Biolabs (Ipswich, MA).

Plasmid construction

The plasmids and primers used in this study are summarized in Tables S1 and S2, respectively. Plasmid pYD1-mSA(wild-type (WT)) was provided by Sheldon Park (Addgene plasmid #39865; Watertown, MA) (37). The mutation in question is numbered according to the Protein Data Bank file 4JNJ. The pYD1_mSA(S25H) gene was obtained by site-directed mutagenic PCR of the pYD1_mSA(WT) plasmid using primers F1 and R1. Then the mSA(S25H) insert was amplified using primers F2/R2 and subcloned into the pCHA vector that had previously been amplified with primers F3 and R3 via Gibson assembly to generate the C-terminal constructs. To build the constructs for soluble expression in *E. coli*, the mSA(WT) and mSA(S25H) genes were amplified from the pYD1 plasmid using primers F4 and R4. These amplicons were subcloned, via Gibson Assembly, into two pET28 expression vectors (pET28_ybbr-HIS-ELP-FLN and pET28_FLN-ELP-HIS-ybbr) for protein production and purification in *E. coli*. These backbones had been previously amplified with primers F5/R5 and F6/R6, respectively, so that the mSA was attached through its N- or C-terminus to the fourth domain of the *Dictyostelium discoideum* filamin (FLN) fingerprint domain. Additionally, these vectors also contained an elastin-like polypeptide (ELP) flexible linker and histidine and ybbr tags. To create the constructs for surface plasmon resonance (SPR) analysis, the same cloning strategy was used with primers F5/R5 and F4/R4, but the recipient vector only had the FLN domain and the ybbR-His tags (pET28_ybbr-HIS-FLN).

Yeast transformation and culture

The yeast plasmids pYD1_mSA(WT) and pYD1_mSA(S25H) were transformed into *S. cerevisiae* EBY100 yeast strain using a lithium acetate transformation protocol (38). Positive colonies were selected on synthetic defined agar 2% (wt/vol) glucose plates lacking tryptophan (−TRP) and cultivated in −TRP liquid medium containing 2% (wt/vol) glucose at 30°C with shaking (200 rotations per minute (rpm)) to an optical density $(OD)_{600}$ of 8. The cells were washed in ultrapure water before being transferred into fresh −TRP medium supplemented with 0.2% (wt/vol) glucose and 1.8% (wt/vol) galactose to a starting OD_{600} of 0.4 to induce protein expression and display. Induction was carried out at 20°C for 16 h for N-mSA(WT) and 24 h for N- and C-mSA(S25H). Afterwards, the cells were resuspended in phosphate-buffered saline (PBS) (137 mM NaCl, 2.7 mM KCl, 10 mM Na_2HPO_4, 1.8 mM KH_2PO_4 (pH 7.2)) and stored at 4°C for up to 3 weeks.

Flow cytometry

Four million cells were added to each well together with 100 μL of 0.1% (wt/vol) bovine serum albumin (BSA) in PBS and pelleted. The supernatant was discarded, and cells were washed with 200 μL of PBS 0.1% (wt/vol) BSA. Incubation with 100 μL of anti-FLAG or anti-hemagglutinin (HA) primary antibody (1:500 dilution) was carried out at room temperature for 30 min. Then the cells were pelleted and washed twice with 200 μL of 0.1% (wt/vol) BSA in PBS. Yeast cells were then labeled with goat anti-mouse secondary antibodies conjugated with Fluorescein isothiocyanate (FITC) or AlexaFluor 594 (1:500 dilution) in the same volume used for the first antibody labeling, for 20 min. For the biotin labeling, yeast cells were incubated in 400 μM of biotin-Atto565 for 30 min. After labeling, cells were washed three times with 200 μL of 0.1% BSA (wt/vol) in PBS and then resuspended in 200 μL and analyzed via flow cytometry.

Protein production and purification in *E. coli*

mSA(S25H) and mSA(WT) constructs for AFM and SPR experiments were transformed into *E. coli* BL21(DE3) cells. Positive colonies were selected in Lysogeny broth (LB)-agar plates supplemented with ampicillin overnight at 37°C. A single colony was used to inoculate LB medium supplemented with kanamycin (LB-Kan) and grown overnight at 37°C with shaking. This preculture was used to inoculate 500 mL of LB-Kan and incubated at 37°C with shaking until OD_{600} reached 0.6. Protein expression was then induced with 0.5 mM of

isopropyl-β-D-1-thiogalactopyranoside overnight at 18°C with shaking. Cells were harvested by centrifugation, resuspended in lysis buffer (50 mM Tris, 50 mM NaCl, 0.1 mg/mL lysozyme, 2 U/mL of DNaseI (pH 8)), and incubated on ice for 15 min followed by sonication. Cell lysate was centrifuged at 18,000 $\times$ *g* for 30 min at 4°C. All proteins were purified by histidine-tag affinity chromatography with a His-Trap FF column using a GE-AKTA chromatography system (GE Healthcare, Chicago, IL). Endogenous biotin was removed by heating the purified proteins to 75°C, followed by buffer exchange into PBS at 40°C. The purified proteins were analyzed by electrophoresis on a 12% sodium dodecyl sulfate–polyacrylamide gel for purity and correct molecular weight. Protein concentration was estimated by absorbance at 280 nm.

SPR

SPR measurements were conducted on an SR7500DC instrument (Reichert Technologies, Depew, NY). In preparation for the experiment, the system was initially flushed twice with 0.5% (m/m) SDS solution, followed by glycine hydrochloride (50 mM (pH 9.5)), and finally ultrapure water. A carboxymethyldextran chip (Xantec, CMD200M; Düsseldorf, Germany) was installed, and the system was equilibrated for 20 min with running buffer (PBS (pH 7.2)). The chip surface was activated for 5 min at 10 μL min^{-1} with a freshly prepared solution of 0.23 M 1-Ethyl-3-(3-dimethylaminopropyl)carbodiimide (EDC) and 0.095 M *N*-hydroxysuccinimide (NHS), followed by immobilization of 100 μM NH_2-Polyethylene glycol (PEG)-biotin (5kDa, Rapp Polymere, Tübingen, Germany) for 20 min. The remaining active carboxylic acid groups were blocked with ethanolamine hydrochloride (1 M (pH 9.5)) for 5 min, and the system was afterwards flushed with five injections of PBS in preparation for the kinetic analysis. Binding kinetics were measured in four subsequent cycles for each protein construct, in each of which the analyte (mSA(WT) or mSA(S25H)) was injected at a different concentration (0.5, 1, 2.5, and 5 μM) in order of increasing molarity. Each cycle comprised a 30 μL $\cdot$ min^{-1} injection of PBS for 5 min, followed by analyte association and dissociation phases, then a PBS injection at 30 μL $\cdot$ min^{-1} for 5 min and a final regeneration step with 0.1 M NaOH at a flow rate of 50 μL $\cdot$ min^{-1} for 2 min. The raw data were extracted and analyzed with Origin (OriginLab Corporation, Northampton, MA). Dissociation curves were fitted globally, taking into account the baseline offset R_0, with Eq. 1, to extract the dissociation constant (k_{off}) and respective standard error.

$$f(t) = (R_{max} - R_0) \times e^{(-k_{off} \times t)} + R_0 \quad (1)$$

The association constant (k_{on}) is reported as the average of the association constants extracted by fitting each association curve with Eq. 2, using the previously determined dissociation constant (k_{off}) as a fixed parameter.

$$f(t) = \frac{(R_{max} - R_0)[A]}{\left(\frac{k_{off}}{k_{on}}\right) + [A]} \times 1 - e^{(-k_{off} \times t)} + R_0 \quad (2)$$

The reported K_D is an average of the K_D-values calculated using the association constants extracted above for each curve and the fixed k_{off}. Errors reported for k_{on} and K_D are standard deviation from the mean.

Silanization of coverslips and cantilevers

AFM cantilevers (BioLever Mini BL-AC40TS; Bruker, Billerica, MA) were cleaned by ultraviolet-ozone treatment. 25 mm glass coverslips (Menzel Gläser, Thermo Fisher Scientific) were sonicated in 50% ethanol for 15 min, rinsed with water, and incubated in piranha solution (1:1 H_2SO_4 (concentrated):H_2O_2 (30%) (v/v)) for 30 min, followed by extensive washing with ultrapure water. Surfaces were then incubated in 2% (v/v) 3-aminopropyl(diethoxy)methylsilane (ABCR GmbH, Karlsruhe, Germany) in a solution of 88% (v/v) ethanol and 10% (v/v) water for 1 h with shaking (coverslips) or 5 min (cantilevers). Subsequently, the coverslips were washed in ethanol and ultrapure water, and cantilevers were washed in toluene, ethanol, and ultrapure water. Surfaces were then dried at 80°C for 30 min.

Spinning disk adhesion assay

The spinning disk apparatus was adapted from previously described designs (20,39) and built in house as reported previously (21).

Aminosilanized coverglasses were functionalized with 25 mM NHS-PEG-biotin (5 kDa; Rapp Polymere, Tübingen, Germany) in 100 mM HEPES buffer for 30 min, washed with ultrapure water, and then blocked with 5% BSA in PBS for 30 min. Yeast cells expressing mSA(WT) or mSA(S25H) were seeded on the surface and allowed to adhere for 30 min at room temperature. Before spinning, the cell suspension was removed and gently replaced with PBS. The coverslips were mounted on the spinning disk device, secured by vacuum suction, and immersed in a solution of PBS at room temperature. The spinning routine consisted of a 20 s acceleration ramp, 5 min steady spinning at the indicated rpm value, and 20 s deceleration. During the adhesion assay, the coverslips were maintained at a height of 25 mm from the bottom of the chamber to minimize turbulence and not disrupt the laminar boundary layer. The shear stress (τ; Pa) at any point on the surface of the coverglass varies linearly with radial distance and is described by the following equation,

$$\tau = 0.800 r \left(\rho \mu \omega^3\right)^{1/2}, \quad (3)$$

where *r* is the radial position relative to the center of the coverglass, ρ is the spinning buffer density, μ is the fluid dynamic viscosity, and ω is the rotational speed (18). After spinning, the coverglasses were raster scanned and imaged frame by frame at 10$\times$ magnification on an Olympus IX81 microscope ($\sim$500 individual images automatically stitched together with CellSens software (version 1.16; Olympus, Tokyo, Japan)) and saved in TIFF format. We used a custom Python-based image analysis script that takes as input the TIFF files, finds the outer circle of the coverglass, and then segments the cells from the background by gray-value thresholding. The script returns the radius of the coverglass and a list containing the area, *XY* coordinates, and distance to the center of the coverglass for every cell detected. Further analysis was performed in MATLAB 2019a (The MathWorks, Natick, MA). The fraction of adherent cells (*f*) at different positions on the disk was calculated by normalizing the density of cells at each section of the disk with the density of cells at the center of the disk, where the shear forces are close to zero. We plotted the detachment profiles (*f* vs. τ) and fitted them with a sigmoid probabilistic model (40):

$$f = 1/(a - exp\,[b\,(\tau - \tau_{50})]), \quad (4)$$

where τ_{50} is the shear stress at which 50% of the cells remain adherent. This value was used as a measure of mean adhesion strength for comparison of cell populations.

Force spectroscopy surface preparation

Aminosilanized coverglasses were functionalized with 10 mg/mL sulfosuccinimidyl 4-(N-maleimidomethyl)cyclohexane-1-carboxylate

(Thermo Fisher Scientific) in 50 mM HEPES for 30 min, followed by incubation with coenzyme A (200 μM) in coupling buffer (50 mM sodium phosphate, 50 mM NaCl, 10 mM EDTA (pH 7.2)) for 1 h. The ybbR tag of the purified constructs was then used to couple these to coenzyme A in the coverglasses in an SFP phosphopantetheinyl transferase-catalyzed reaction in PBS buffer at room temperature for 2 h. Silanized cantilevers were incubated with 25 mM NHS-PEG-Biotin (5 kDa; Rapp Polymere) in 100 mM HEPES buffer for 30 min and washed with ultrapure water. Functionalized cantilevers and coverglasses were kept in PBS until the measurement.

Force spectroscopy measurements

Force spectroscopy measurements were carried out using an automated AFM-based force robot (Force Robot 300; JPK Instruments, Berlin, Germany), in PBS buffer, at room temperature under varying pulling velocities. The cantilever was calibrated using the thermal noise method. Loading rates were estimated by a line fit to the force versus time trace immediately before the rupture event. During the experiment, a loose filter was set for curves with 3–6 peaks, rupture forces under 500 pN, and a tip-sample separation at rupture of $>$30 nm to distinguish traces with and without interactions. Force versus piezo position curves meeting these criteria were then processed by baseline subtraction, adjustment of x-offset, and extension correction to account for cantilever bending. The force versus molecular extension traces were then transformed into contour length using the worm-like chain model (2,41). Curves were manually selected by searching for a contour length increment that matched the FLN fingerprint domain unfolding events, which added $\sim$32 $\pm$ 8 nm of hidden contour length to the system. Additionally, only traces showing a minimal contour length of 90 nm before FLN unfolding were considered; this corresponds to the length of the stretched PEG linker and ELP present in the pulling configuration during retraction of the cantilever. Subsequent analysis was performed in MATLAB 2019a. The histograms of the rupture force for the complex for each pulling speed were fitted with the Bell-Evans model (42) to determine the most probable rupture force and loading rate. Finally, a linear fit was performed through the most probable forces and most probable loading rates at the different pulling speeds to determine the distance to the transition state (Δx) and the off rate at zero force (k_{off}). Reported errors in Fig. 2, *E* and *F* represent the asymmetric full width at half maximum for each probability distribution.

RESULTS

Equilibrium kinetic binding constants of mSA(WT) and mSA(S25H)

We first sought to validate the equilibrium kinetic parameters reported previously for mSA(WT) and mSA(S25H) using SPR. Genes encoding mSA were cloned into a pET28 expression vector containing C-terminal ybbr and hexahistidine tags and overexpressed in *E. coli*. The two protein constructs mSA(WT) and mSA(S25H) were then purified via metal-ion chromatography and transferred to PBS. SPR measurements were carried out by sequentially injecting solutions of mSA(WT) and mSA(S25H) at different concentrations over a biotin-functionalized carboxymethyldextran-gold chip. Specific association of mSA to the immobilized biotin produced a rise in the SPR signal, which then decreased during the dissociation phase. For each construct, dissociation curves were fitted (Eq. 1) to extract the dissociation constant (k_{off}) and with a fixed k_{off}, the association curves were fitted with Eq. 2 to extract the association constant (k_{on}). The calculated kinetic parameters are summarized in Table 1. The measured k_{off} of mSA(S25H) was found to be (0.47 $\pm$ 0.05) $\times$ 10^{-3} s^{-1}, which was $\sim$10-fold lower than that of mSA(WT) (5.44 $\pm$ 0.02) $\times$ 10^{-3} s^{-1}. This result is consistent with prior experiments and molecular dynamics simulations, which showed that the S25H mutation can shield the binding pocket of mSA from the bulk solvent, reduce flexibility of the L3,4 loop (residues 45–51), and enhance binding (12). We found that both constructs exhibited similar association constants of (65.25 $\pm$ 1.22) $\times$ 10^3 M^{-1} s^{-1} for mSA(S25H) and (41.58 $\pm$ 0.96) $\times$ 10^3 M^{-1} s^{-1} for mSA(WT). Subsequently, the equilibrium dissociation constants (K_D) were determined as 7.42 $\pm$ 1.57 nM for mSA(S25H) and 137 $\pm$ 29 nM for mSA(WT).

Regarding k_{off}, our results are in close agreement with those reported before. However, the previous study reported similar K_D-values for both mSA(WT) and mSA(S25H), whereas here we report a 19-fold difference in K_D. Additionally, we report 10 to 100-fold higher absolute K_D-values in this study than those reported by Park and colleagues (12). We attributed these differences to the different methods used to measure the binding affinity, as in the other study this constant was estimated through a measurement on the yeast surface, whereas here, we performed SPR using *E. coli* purified proteins immobilized on a chip. Overall, our results support the claim that the mSA(S25H)-biotin complex has a $\sim$10-fold lower off rate than mSA(WT)-biotin and 10 to 30-fold lower K_D.

Comparison of N- and C-terminal pulling geometries using AFM-SMFS

We used AFM-SMFS to evaluate whether mSA(WT)-biotin and mSA(S25H)-biotin complexes show the same trends in mechanical stability as in equilibrium affinity measurements (Fig. 1, *left*). For SMFS, in addition to the mSA receptor, we included the fourth domain of the *Dictyostelium discoideum* F-actin cross-linking protein filamin (FLN) as a fingerprint domain designed to unfold before rupture of the biotin-mSA interaction. FLN was further fused to an ELP sequence and a His-ybbR tag (43) (Fig. 2 *A*). The ELP served as an intrinsically disordered flexible linker that exhibits uniform entropic stretching behavior in AFM-SMFS and therefore provides better agreement with standard polymer elasticity models such as the worm-like chain when compared with the more common PEG-linkers (44,45). The ybbR tag was used to covalently attach the constructs to a coenzyme-A-functionalized coverglass at the N-terminus

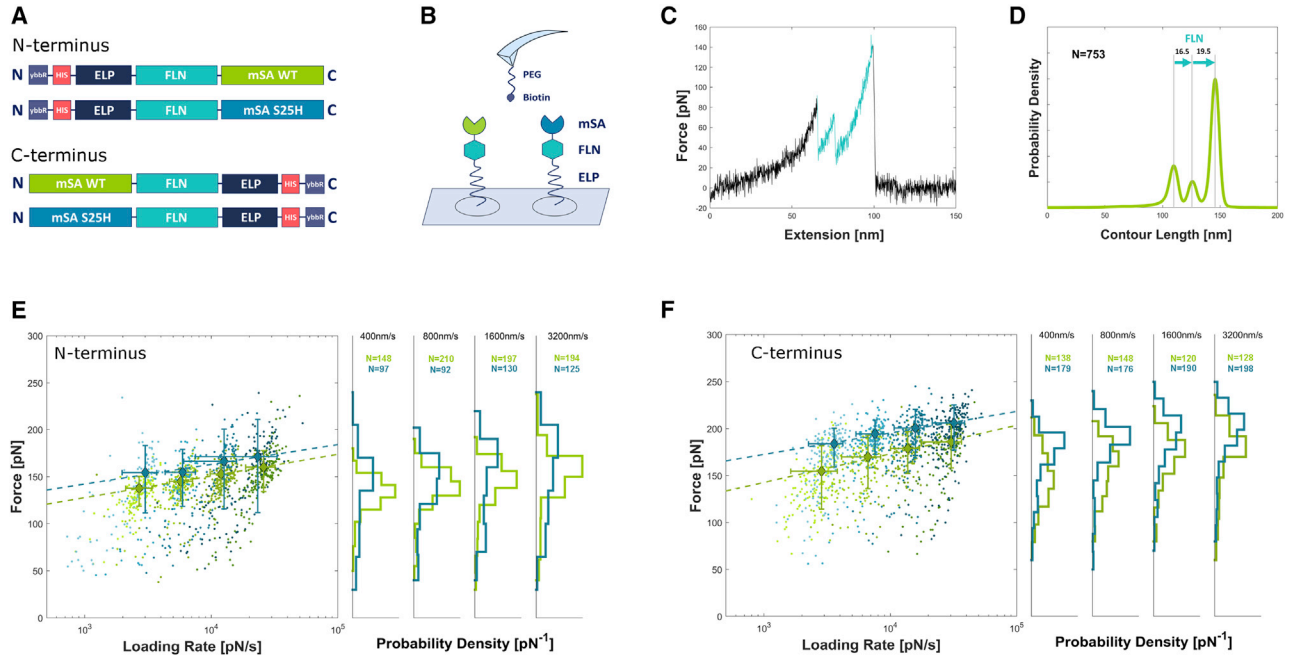

FIGURE 2 Mechanical stability of mSA(WT)-biotin and mSA(S25H)-biotin complexes. (*A*) Gene cassettes used for mSA expression in *E. coli* before AFM-SMFS. (*B*) Pulling configuration of the SMFS measurement with biotin attached to the cantilever and the two mSA protein constructs immobilized at different spots on the surface. (*C*) Example of a typical force versus extension trace showing unfolding of FLN in two steps followed by rupture of the biotin/N-mSA complex at a pulling speed of 400 nm/s. (*D*) Contour length histogram obtained from n = 753 single-molecule dissociation curves of N-mSA(WT)/biotin complexes, similar to the trace shown in (*C*). (*E* and *F*) Dynamic force spectra of , respectively, N-terminal and C-terminal anchor points for mSA(WT)-biotin (*green*) and mSA(S25H)-biotin (*blue*) complex rupture events obtained at pulling speeds of 400, 800, 1600, and 3200 nm/s. Colored dots represent individual rupture events. Diamond markers represent the most probable rupture force and loading rate values for each pulling speed. The dashed line represents the Bell-Evans model fits to the diamond markers. Error bars are full width at half maximum for each rupture force and loading rate distribution (*left*). Overlapping rupture force histograms obtained at each pulling speed for mSA-biotin complex rupture events are shown (*right*). N shows the number of individual rupture events considered in each histogram. Data for the N- and C-terminal constructs were acquired in separate experiments. In the experiment for the C constructs, the N-S25H protein was used as an internal control (Fig. S3).

via 4′-phosphopantetheinyl transferase-mediated ligation. mSA(WT) and mSA(S25H) were fused with FLN such that mSA was attached either by its N- or C-terminus. The four proteins are denoted as follows:

1) ybbR-His-ELP-FLN-mSA(WT) (N-WT).
2) ybbR-His-ELP-FLN-mSA(S25H) (N-S25H).
3) mSA(WT)-FLN-ELP-His-ybbR (C-WT).
4) mSA(S25H)-FLN-ELP-His-ybbR (C-S25H).

Mechanical dissociation of the mSA-biotin complexes was probed with PEG-biotin covalently immobilized on the cantilever and the fusion proteins covalently attached to the coverglass. The mSA(WT) and mSA(S25H) constructs were immobilized at different locations on the same coverglass surface and probed with the same cantilever for each pulling geometry (C- or N-terminal pulling) (Fig. 2 *B*). The biotin-functionalized cantilever tip was lowered to the mSA proteins immobilized on the surface, allowing an mSA-biotin receptor-ligand complex to form. The cantilever was then retracted, and, if a complex was successfully formed, the force-extension trace exhibited a pattern corresponding to unfolding of FLN followed by the rupture of the mSA-biotin complex. The FLN fingerprint domain unfolds at relatively low forces (60–100 pN) and displays a characteristic two-step unfolding pattern (46) that distinguishes nonspecific adhesion in SMFS traces from specific pulling on individual mSA-biotin complexes to validate and identify single-molecule interactions. A typical force-extension trace (Fig. 2 *C*) showed unfolding of FLN in two steps followed by rupture of a single mSA-biotin complex. In some cases, FLN unfolded in a single step before the rupture of the mSA-biotin complex. In such cases, the contour length increment observed corresponded to that of the full FLN domain (∼32 nm) (Fig. S2).

The SMFS measurement was performed at four different pulling speeds (400, 800, 1600, and 3200 nm/s) to estimate the energy landscape parameters. Based on the minimal contour length requirement and the FLN unfolding pattern, single-molecule curves were screened for specific mSA-biotin interactions. We analyzed the final rupture events from the selected curves obtained at the four pulling speeds and

TABLE 1 SMFS, SPR, and SDA calculated parameters

	SMFS						SPR			SDA
	Most probable rupture force (pN)				Landscape parameters					
Samples	400 nm/s	800 nm/s	1600 nm/s	3200 nm/s	Δx (nm)	Ln k_0	k_0 (s^{-1})	k_{on} (10^3 M^{-1} s^{-1})	k_{off} (10^{-3} s^{-1})	K_D (nM)	τ_{50} (dyn · cm^{-2})
N-WT	138	145	153	160	0.41 ± 0.01	−8.14 ± 0.26	2.92×10^{-4}	41.58 ± 0.96	5.44 ± 0.02	137.41 ± 28.90	118.48 ± 7.11[a]
N-S25H	154	155	166	171	0.45 ± 0.10	−10.92 ± 3.78	1.81×10^{-5}	65.25 ± 1.22	0.47 ± 0.05	7.42 ± 1.57	112.60 ± 10.41[b] 196.10 ± 5.89[a], 189.20 ± 6.16[b]
C-WT	155	170	179	186	0.31 ± 0.04	−6.48 ± 1.43	1.53×10^{-3}	N/A	N/A	N/A	N/A
C-S25H	184	195	201	206	0.41 ± 0.05	−12.76 ± 2.15	2.87×10^{-6}	N/A	N/A	N/A	185.32 ± 8.25[b]

Most probable rupture forces (for errors, see Fig. 2, *E* and *F*) obtained at varied pulling speeds and energy landscape parameters based on the Bell-Evans model (errors are standard error of the parameters computed by the fit). Kinetic parameters were determined via SPR: errors for k_{on} and K_D are standard deviation from the mean, and error for k_{off} is standard error from fit extracted value. SDA adhesion strength was calculated based on a sigmoid model (errors are 95% confidence intervals). N/A, not applicable.

[a]τ_{50} calculated from the multiple speed measurement presented in Fig. 3 *D*.

[b]τ_{50} calculated from the single speed measurement presented in Fig. 3 *E* and Fig. S5.

generated histograms describing the rupture force distributions of mSA-biotin unbinding for both mSA(WT) and mSA(S25H) in both N-terminal (Fig. 2 *E*) and C-terminal (Fig. 2 *F*) pulling geometries. The rupture force distributions indicate that the stabilizing effect of the S25H mutation that was observed in the SPR experiments also manifests when the complex was tested under mechanical tension (Table 1). Generally, the mSA(S25H)-biotin complex exhibited higher rupture forces than mSA(WT)-biotin across the entire range of pulling speeds from 400 to 3200 nm/s for both pulling geometries. The N-mSA(WT)-biotin complex ruptured at forces ranging from 138 to 160 pN at loading rates of 10^3–10^4 pN/s, whereas the N-mSA(S25H)-biotin ruptured at 154–171 pN. For the C-terminal constructs, the rupture forces ranged from 155 to 186 pN for the C-mSA(WT) complex and 184–206 pN for the C-mSA(S25H) mutant. The higher mechanostability of mSA(S25H)-biotin complexes was consistently observed across the four pulling speeds and for both pulling geometries, as well as in independent replicates (n = 3). Furthermore, higher rupture forces were observed for both the WT and S25H C-terminal constructs when compared with the N-terminal pulling geometry (Fig. 2, *E* and *F*; Fig. S3; Table 1).

To determine a simplified energy landscape for the unbinding reaction under force, we investigated the loading rate dependency of the mSA-biotin rupture events. We plotted the unbinding forces as a function of the loading rate and analyzed the results using the phenomenological Bell-Evans model (42). From the linear fit of the most probable rupture force versus the most probable loading rate at each pulling speed for N- (Fig. 2 *E*, *left*) and C-terminal (Fig. 2 *F*, *left*) pulling configurations, we obtained estimates for Ln(k_0) and the distance to the transition state along the reaction coordinate (Δx) (Table 1). We note that k_{off}-values from Bell-Evans fitting procedures can vary widely because of extreme model sensitivity (47), especially when a narrow range of loading rates is tested as is the case here, although trends in Δx-values are typically more robust. Nonetheless, Ln(k_0)-values for both N- and C-terminal-anchored mSA(S25H) (N-S25H −10.92 ± 3.78; C-S25H −12.76 ± 2.15) were found to be lower than those of N- and C-terminal mSA(WT), respectively (N-WT −8.14 ± 0.26; C-WT −6.48 ± 1.43), a qualitative trend that was consistent with the SPR data. We further note it is not assumed the k_{off}-values between SMFS and SPR are expected to quantitatively agree because they are probing separate reaction pathways and the force-based measurement is extrapolated to zero force. In terms of the Δx parameter, the N-terminal constructs both have a similar barrier position and therefore a similar sensitivity to loading rate, with values of Δx = 0.41 ± 0.01 nm for

N-WT and $\Delta x = 0.45 \pm 0.10$ nm for N-S25H. However, in the case of the C-terminal constructs, mSA(WT) exhibits a steeper loading rate dependency (i.e., shorter barrier position ($\Delta x = 0.31 \pm 0.04$ nm) in relation to mSA(S25H) ($\Delta x = 0.41 \pm 0.05$ nm). Together, these results suggest different levels of mechanostability and different unbinding pathways for the two mSAs in this study, which is consistent with the predicted changes produced by the S25H mutation.

S25H mutation imparts higher adhesion in SDA

We hypothesized that mSA variants that form more mechanostable interactions with biotin as measured by AFM-SMFS would also mediate stronger cell adhesion to biotinylated surfaces under flow. We therefore developed an SDA protocol that allowed us to evaluate the adhesion strength of yeast cell populations displaying mSA to biotinylated coverglass surfaces (Fig. 1, *right*).

For the purpose of yeast surface display of proteins, yeast a-agglutinin subunit 2 (Aga2p) is linked by two disulfide bridges to Aga1p, a β-1,6-glucan-anchored protein. The co-expression of Aga1p with Aga2p fused to the protein of interest leads to cell wall-anchored proteins on the surface of the yeast.

S. cerevisiae EBY100 cells were transformed with yeast vectors containing mSA(WT) or mSA(S25H) genes in frame with Aga2p as either an N- or C-terminal fusion.

The gene cassettes also contained an HA tag at the N-terminus of mSA and a FLAG tag at the C-terminus. *S. cerevisiae* presents clear advantages in the development of this assay when compared with other display systems. Specifically, the rigid cell wall and relatively large cell size compared to bacterial systems facilitated uniform shearing and straightforward imaging by light microscopy. The lack of cellular appendages and ease of genetic manipulability of yeasts facilitated the application of mechanical forces to analyze molecular interactions of recombinant synthetic receptor proteins with surface-immobilized ligands (29). Furthermore, yeast cells are capable of eukaryotic expression and processing and present quality control mechanisms of the eukaryotic secretory pathway, broadening the number of biomolecular pairs that can be studied with this approach.

After induction, the correct translocation and anchoring of the Aga2 fusion proteins to the yeast cell wall was verified with fluorescent antibody or fluorescent biotin labeling in conjunction with analytical flow cytometry. For both N-WT and N-S25H constructs, $\sim$80% of yeast cells in the population were fluorescently labeled via the FLAG tag at the C-terminal end of the constructs, which indicated a positive display of the proteins of interest (Table S4). However, for the C-terminal configurations, labeling via the HA tag at the end of the constructs showed that only the S25H mutant was successfully displayed (over 80%). The C-WT construct was not able to be successfully displayed despite numerous attempts under varied induction conditions; therefore, this construct was omitted from the SDA analysis.

The display level of each construct was analyzed to account for differences in adhesion profiles that could arise because of different levels of protein at the surface of the cells. The results showed a very similar expression level (Fig. 3 *A*), with the median of fluorescence for the yeast expressing N-S25H being only $\sim$4% higher than that for the population expressing N-WT. Regarding the N- and C-S25H yeast populations, we compared the amount of protein at the surface with the HA tag. The flow cytometry analysis showed that the population histograms for both constructs significantly overlap, with a $\sim$6% higher display level for C-S25H (Fig. 3 *B*). Based on factors such as cell life cycle and inherent variability, these small differences in display levels for the compared constructs were considered negligible. Additionally, we labeled N-S25H and C-S25H with a biotinylated fluorophore, and this yielded a 24% higher median for the N-S25H population with a significant overlap between the histograms for the two populations (Fig. S4). The larger difference in biotin binding for N-S25H versus C-S25H could be due to steric accessibility of the biotin binding pocket that influences the on rates.

Adhesion profiles for a given cell population were obtained by first allowing the cells to settle and bind to a covalently biotinylated coverglass. Next, a gradient of hydrodynamic shear stress was applied by spinning the disk submerged in buffer at a given rotational speed (3000–5000 rpm). As the disk spins, the fluid approaches the disk surface and acquires a rotational motion that then forces it radially outward, causing the bonds between the immobilized ligand and the proteins displayed on cells to be mechanically strained. Cells are removed from the coverglass if the shear stress applied is too high for the molecular bonds to stay bound. In a typical adhesion profile, the number of cells that remain attached decreases with increasing shear stress, which grows linearly with the distance from the center of the disk. The proportion of cells remaining as a function of the shear stress is then fitted with a sigmoidal curve. From this fit, the mean cell detachment shear stress (τ_{50}) can be calculated and represents the adhesion strength for the cell population under the given experimental conditions.

The specificity of the interaction between the yeast cells expressing mSA and the biotinylated surface was first demonstrated by a blocking assay, in which N-WT cells that were previously incubated with 80 μM of free biotin were seeded and spun on the disk. Under the same experimental conditions, only 2% of the

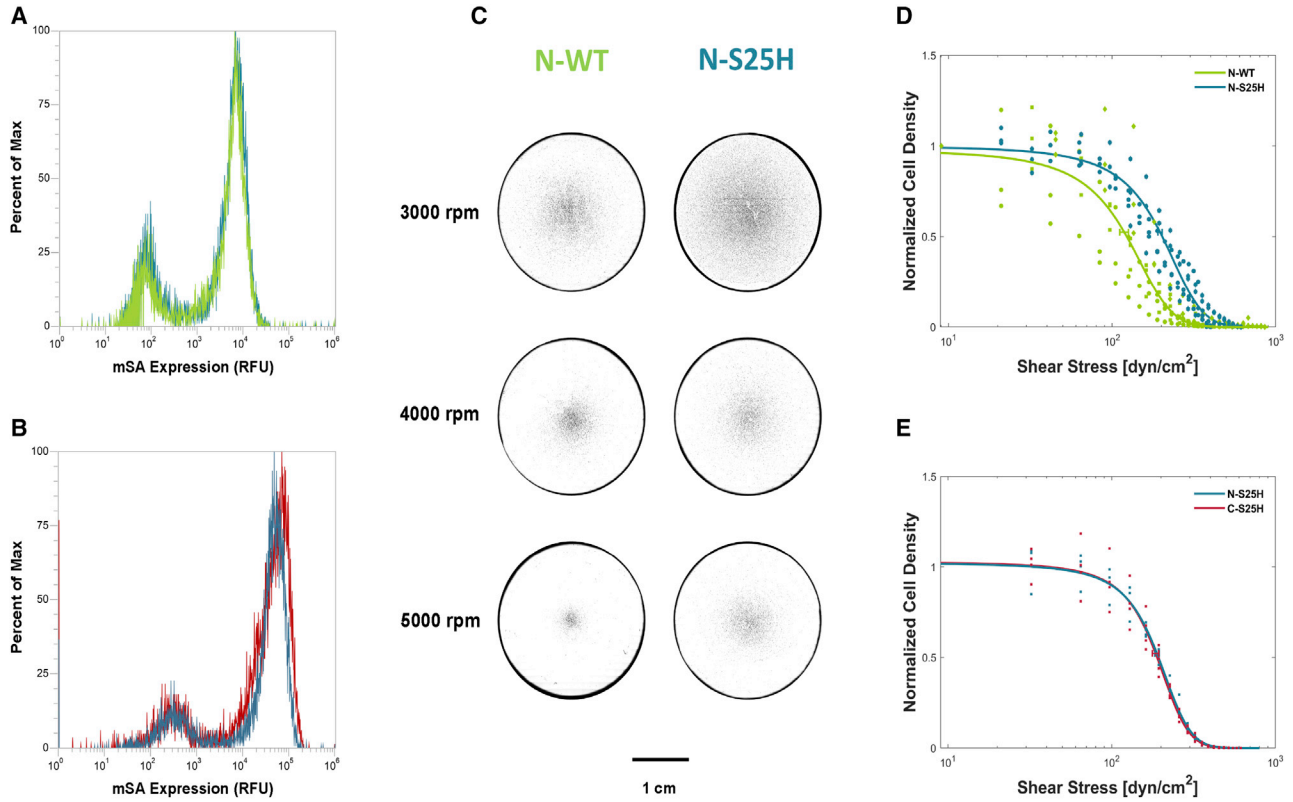

FIGURE 3 Population-level adhesion for mSA(WT) and mSA(S25H). (*A*) Flow cytometry overlapping histograms of yeast cell populations displaying mSA(WT) in green and mSA(S25H) in blue, labeled with anti-FLAG-tag antibody and anti-mouse fluorescein. (*B*) Flow cytometry overlapping histograms of yeast cell populations labeled with anti-HA-tag antibody and anti-mouse AlexaFluor594 displaying N-mSA(S25H) in blue and C-mSA(S25H) in red. (*C*) Segmented images of disks after spinning for the cell populations expressing either N-WT or N-S25H mSA at multiple spinning speeds. (*D*) Cell density versus shear stress plots for N-WT (*green*) and N-S25H mSA (*blue*) yeast populations at 3000 rpm (*circles*), 4000 rpm (*squares*), and 5000 rpm (*diamonds*). Plotted data represent three independent experiments, with each data set containing data from all spinning speeds; the experimental points for each cell population were fitted with a sigmoid model (N-WT $R^2 = 0.87965$; N-S25H $R^2 = 0.94973$), and error bars represent the 95% confidence interval of the τ_{50} calculated by the global fit. (*E*) Cell density versus shear stress plots for N-S25H (*blue*) and C-S25H mSA (*red*) yeast populations at 4000 rpm. Plot shows data from four technical replicates for each population. The experimental points for each cell population were fitted with a sigmoid model (N-S25H $R^2 = 0.98935$; C-S25H $R^2 = 0.97941$), with error bars representing the 95% confidence interval of the τ_{50} calculated by the global fit. RFU, relative fluorescence units.

biotin-blocked cells remained on the disk after spinning, as compared with 50% of nonblocked cells (data not shown).

To obtain adhesion profiles for the N-mSA(WT) and N-mSA(S25H) populations, 10^6 yeast cells were allowed to settle for 30 min onto a biotin-functionalized coverglass blocked with BSA. Before spinning, a gentle wash step with PBS was performed. Each population was studied using a range of spinning speeds. After spinning, the coverglasses were imaged and the adherent population was calculated based on the area occupied by cells in concentric sections of the disk. The cell density in each concentric region was then normalized to the cell density at the center of the disk, where the shear stress is close to zero. Fig. 3 *C* shows that as the spinning speed and consequently the shear stress increased, the number of cells remaining on the outer edges of the disk decreased. Moreover, it was observed that for the same speed, the density of mSA(S25H) cells on the edge of disks after spinning was higher than that of the mSA(WT) population.

The images were then processed to obtain the distance of each cell to the center of the coverglass and enable the plotting and fitting of the adhesion profile. The adhesion profiles of each cell population at varying spinning speeds were fitted by a global sigmoidal function (Fig. 3 *D*; $R^2 > 0.7$ (40)). The noticeable rightward shift of the adhesion profile for N-S25H with respect to the N-WT cell population indicated a higher shear stress was required to detach the cells. This shift also translated into an adhesion strength (τ_{50}) of 196.10 ± 5.89 dyn $\cdot$ cm^{-2} for the N-S25H cells, whereas for N-WT, the τ_{50} was 118.48 ± 7.11 dyn $\cdot$ cm^{-2}. This represented a 40% increase in the adhesion strength of the mutant mSA population when compared with the WT, which was consistent with the trend observed in the AFM-SMFS assays in which S25H exhibited higher rupture forces.

Previous SDAs using mammalian cells reported that although the midpoint cell density shifted toward the center of the disk at higher spinning speeds, the calibrated mean cell detachment shear stress remained the same (18,20). This means that the same τ_{50}-value is expected regardless of the particular speed used. Here, we found the same, specifically that the shift of the detachment profile was visible in the microscope images for different speeds (Fig. 3 *C*), but the variability in the values for τ_{50} was independent of the spinning speed.

We were therefore able to adapt the SDA to study yeast cell adhesion mediated solely by recombinant protein receptors expressed at its surface. The results show that the same trend in mechanostability found in the SMFS-AFM measurements was observable in both SPR and SDA assays. The mSA(S25H)-biotin interaction exhibited higher single-molecule rupture forces and also higher adhesion strength in the SDA when compared with the mSA(WT)-displaying cells.

We sought to understand whether the differences observed due to the different pulling geometry in the AFM-SMFS assay would replicate in the SDA. Several studies have reported differences in mechanical strength of protein complexes depending on the pulling points at which tension is applied in an SMFS measurement (5–7). Because it was not possible to express the C-terminal-anchored construct of the WT construct to a sufficient degree to allow SDA experiments, only the mSA(S25H) populations were tested. The difference between the rupture forces for these two constructs in SMFS (30–50 pN) was larger than the differences detected between the WT and S25H mutant in both pulling geometries (10–35 pN); therefore, we expected to observe a difference in the adhesion strength between N-S25H and C-S25H on the SDA. However, no differences were found between the two pulling geometries in the adhesion assay (Fig. 3 *E*) after repeated testing, despite similar protein expression levels. The adhesion strength was estimated at 189.20 ± 6.16 dyn $\cdot$ cm^{-2} for the N-terminal mSA(S25H) and 185.32 ± 8.25 dyn $\cdot$ cm^{-2} for the C-terminal geometry. As an internal experimental control, N-WT-expressing cells were also tested during this experiment and showed the same trend as seen above when compared with the N-S25H (Fig. S5). Furthermore, this result was observed in independent replicates ($n = 4$). We further analyzed the adhesion strength of cells collected at different induction time points, with increasing amounts of protein on the surface, against the median detected by flow cytometry, which showed similar linear trends for both constructs (Fig. S6). The consistency in results between SMFS and SDA was therefore found to hold when comparing mutant versus WT constructs of the same anchor domain topology (N- versus C-terminal fusion) but did not hold when the topology was changed.

DISCUSSION

A number of experimental techniques are available to study the mechanical properties of protein interactions, and the topic is of broad interest in protein engineering and mechanobiology. In this study, we compared three methods with which it was possible to quantify the binding strength of receptor-ligand interactions: SPR, SMFS, and SDA. We found that the mSA mutant S25H, which exhibits lower k_{off} and lower K_D, also leads to higher rupture forces of the mSA-biotin complex in SMFS experiments in both N- and C-terminal pulling geometries. Although the differences found between WT and S25H mSA on AFM were relatively small (10–35 pN), the results were consistent across four pulling speeds and in both pulling geometries. Moreover, the C-terminal attachment of mSA yielded higher rupture forces than the N-terminal anchoring geometry, with a difference of 30–50 pN. This anchor geometry effect was in line with previous data obtained with a monovalent streptavidin tetramer, in which the rupture force for the streptavidin monomer attached through the C-terminus was twofold higher than for its N-terminal counterpart (7). Another study that looked at the differences between the N- and C-terminal geometries of another mutant mSA (T48F) also found the interaction to be ~30–40 pN stronger for geometry C than for geometry N (5).

We successfully adapted the SDA to investigate the mechanical stability of the interaction between mutant or WT mSA and biotin by quantifying the adhesion profiles under shear stress for yeast populations displaying different recombinant mSA receptors. The results for N-WT and N-S25H were found to correlate with those obtained by SMFS and SPR, with N-S25H exhibiting a higher rupture single-molecule force and also mediating stronger adhesion of the cells to the biotinylated surface than N-WT. Furthermore, we attempted to draw the same correlation when comparing N- and C- terminal pulling geometries. In the SMFS measurements, the rupture forces for the C-terminal S25H were significantly higher than N-terminal S25H. However, this trend could not be observed in the SDA assay. The correlation between cell population adhesion strength and single-molecule receptor-ligand ruptures was therefore only confirmed when comparing variants of different stability in a fixed anchoring geometry.

We can speculate that differences in the kinetic on rates (k_{on}) that manifest because of the position of the AGA2-fusion domain could account for this observation. Because the SDA can result in rolling cell adhesion, the on rate (k_{on}) could also influence the cell adhesion strength. A lower association rate (k_{on}) for the N-terminal S25H mSA would decrease the cells' ability to form new interactions upon initiation of rolling, leading to easier cell detachment from the disk.

In fact, residue D128, responsible for forming long-lived hydrogen bonds between structural water molecules and biotin in mSA(S25H) (12), is located very close to the C-terminus of mSA. If anchoring or fusing the protein through this end limits the structural flexibility of the molecule in this particular region, we expect the k_{on} parameter could be affected.

The SDA is a highly tunable and adaptable assay that can be applied to many receptor-ligand pairs and does not require particularly sophisticated equipment or expertise to set up. Because of its simplicity and ease of use, it can become a helpful approach to acquire preliminary data on receptor-ligand complexes before SMFS studies are conducted. During the SDA, depending on the shear stress conditions, cells can remain fixed on the disk, enter a rolling adhesion regime, or completely detach. Both on-rate and off-rate kinetic parameters influence the dynamics of bond formation and rupture in the SDA assay (30,48,49), whereas AFM-SMFS probes only the unbinding reaction (i.e., only k_{off}). In considering the lack of correlation when comparing different pulling geometries, very few experimental studies have looked at this correlation. Although SMFS allows us to study quantitatively unbinding energy landscapes in detail, the SDA might in some cases more closely represent the force environment in question and take into account dynamic affinity, dynamic adhesion, and other parameters that influence the interactions in their natural or biotechnological application environment, as is the case for interactions in shear stress environments or in which multivalency plays a role.

We note that differences in glycosylation patterns of proteins expressed in yeast versus bacteria could influence the correlations discussed here, but this needs to be considered on a case-by-case basis, and we do not expect mSA to be highly glycosylated. The applied force per cell has been estimated in previously described SDAs with mammalian cells (40). In SMFS, the loading rate on the single bond is expected to be higher than in the case in the SDA, and this is an additional factor that makes correlations challenging. It is further challenging to account for small differences in avidity, cell size distribution, and varied loading rates for different bonds on the same cell. Additionally, if the cells enter a state of rolling adhesion, the SDA may be influenced by k_{on}, whereas SMFS in the format presented here only probed k_{off}.

Compared to SMFS, the SDA is in many ways a simpler approach to characterize the mechanical stability of biomolecular interactions. This system could be easily adapted to receptor-ligand pairs exhibiting rupture forces much higher than mSA-biotin by simply adjusting the viscosity of the spinning buffer to increase the shear stress applied, by titrating the amount of ligand on the surface of the disk or at the surface of the yeast cells, or by changing rotational speeds. The sensitivity of the SDA can therefore be tuned to receptors of different binding strengths.

Our work highlights the nuances in drawing correlations between single-molecule mechanics and cell adhesion under flow, identifies challenges in quantitatively correlating these behaviors, and opens up new research avenues in screening receptors for adhesion under flow.

SUPPLEMENTAL INFORMATION

Supplemental information can be found online at https://doi.org/10.1016/j.bpr.2021.100035.

AUTHOR CONTRIBUTIONS

Conceptualization and experimental design: M.S.S., R.V., H.L., and M.A.N.; SPR data collection: V.S.; biochemical preparations, AFM-SMFS, flow cytometry, and SDA data collection: M.S.S.; data analysis: M.S.S. and V.S.; analytic tools: M.S.S., V.S., R.V., H.L., and M.A.N.; original draft preparation: M.S.S. and M.A.N.; review and editing: M.S.S., R.V., H.L., V.S., and M.A.N.; supervision and funding acquisition: M.A.N.

DECLARATION OF INTERESTS

The authors declare no competing interests.

ACKNOWLEDGMENTS

The authors thank Gian-Luca Schmid for help in characterizing and optimizing SDA experiments as well as Joanan López Morales for helpful discussions.

This work was supported by the University of Basel, ETH Zurich, an European Research Council Starting Grant (MMA-715207), the National Centre of Competence in Research for Molecular Systems Engineering, and the Swiss National Science Foundation (Project 200021_175478).

REFERENCES

1. Ott, W., M. A. Jobst, …, M. A. Nash. 2017. Single-molecule force spectroscopy on polyproteins and receptor-ligand complexes: the current toolbox. *J. Struct. Biol.* 197:3–12.
2. Yang, B., Z. Liu, …, M. A. Nash. 2020. Next generation methods for single-molecule force spectroscopy on polyproteins and receptor-ligand complexes. *Front. Mol. Biosci.* 7:85.
3. Mora, M., A. Stannard, and S. Garcia-Manyes. 2020. The nanomechanics of individual proteins. *Chem. Soc. Rev.* 49:6816–6832.
4. Sumbul, F., and F. Rico. 2019. Single-molecule force spectroscopy: experiments, analysis, and simulations. *Methods Mol. Biol.* 1886:163–189.
5. Bauer, M. S., L. F. Milles, …, H. E. Gaub. 2018. Monomeric streptavidin: a versatile regenerative handle for force spectroscopy. *bioRxiv* https://doi.org/10.1101/276444.
6. Liu, Z., R. A. Moreira, …, B. Yang. 2021. Optimizing mechanostable anchor points of engineered lipocalin in complex with CTLA-4. *bioRxiv* https://doi.org/10.1101/2021.03.09.434559.

7. Sedlak, S. M., L. C. Schendel, …, R. C. Bernardi. 2019. Direction matters: monovalent streptavidin/biotin complex under load. *Nano Lett.* 19:3415–3421.
8. Durner, E., W. Ott, …, H. E. Gaub. 2017. Post-translational sortase-mediated attachment of high-strength force spectroscopy handles. *ACS Omega.* 2:3064–3069.
9. Otten, M., W. Ott, …, H. E. Gaub. 2014. From genes to protein mechanics on a chip. *Nat. Methods.* 11:1127–1130.
10. Zhou, D. W., and A. J. García. 2015. Measurement systems for cell adhesive forces. *J. Biomech. Eng.* 137:020908.
11. Stern, L. A., C. M. Csizmar, …, B. J. Hackel. 2017. Titratable avidity reduction enhances affinity discrimination in mammalian cellular selections of yeast-displayed ligands. *ACS Comb. Sci.* 19:315–323.
12. Demonte, D., E. J. Drake, …, S. Park. 2013. Structure-based engineering of streptavidin monomer with a reduced biotin dissociation rate. *Proteins.* 81:1621–1633.
13. Humphrey, W., A. Dalke, and K. Schulten. 1996. VMD: visual molecular dynamics. *J. Mol. Graph.* 14:33–38, 27–28.
14. Yakovenko, O., S. Sharma, …, W. E. Thomas. 2008. FimH forms catch bonds that are enhanced by mechanical force due to allosteric regulation. *J. Biol. Chem.* 283:11596–11605.
15. Yakovenko, O., V. Tchesnokova, …, W. E. Thomas. 2015. Inactive conformation enhances binding function in physiological conditions. *Proc. Natl. Acad. Sci. USA.* 112:9884–9889.
16. Li, N., H. Yang, …, M. Long. 2018. Ligand-specific binding forces of LFA-1 and Mac-1 in neutrophil adhesion and crawling. *Mol. Biol. Cell.* 29:408–418.
17. Horbett, T. A., J. J. Waldburger, …, A. S. Hoffman. 1988. Cell adhesion to a series of hydrophilic-hydrophobic copolymers studied with a spinning disc apparatus. *J. Biomed. Mater. Res.* 22:383–404.
18. García, A. J., P. Ducheyne, and D. Boettiger. 1997. Quantification of cell adhesion using a spinning disc device and application to surface-reactive materials. *Biomaterials.* 18:1091–1098.
19. Friedland, J. C., M. H. Lee, and D. Boettiger. 2009. Mechanically activated integrin switch controls $\alpha5\beta1$ function. *Science.* 323:642–644.
20. Fuhrmann, A., and A. J. Engler. 2015. Acute shear stress direction dictates adherent cell remodeling and verifies shear profile of spinning disk assays. *Phys. Biol.* 12:016011.
21. Huo, Z., M. Sá Santos, …, S. J. Gros. 2021. Metastatic esophageal carcinoma cells exhibit reduced adhesion strength and enhanced thermogenesis. *Cells.* 10:1213.
22. Boder, E. T., and K. D. Wittrup. 1997. Yeast surface display for screening combinatorial polypeptide libraries. *Nat. Biotechnol.* 15:553–557.
23. Wang, Z., A. Mathias, …, D. M. Neville, Jr. 2005. A new yeast display vector permitting free scFv amino termini can augment ligand binding affinities. *Protein Eng. Des. Sel.* 18:337–343.
24. Wang, X. X., Y. K. Cho, and E. V. Shusta. 2007. Mining a yeast library for brain endothelial cell-binding antibodies. *Nat. Methods.* 4:143–145.
25. van den Beucken, T., H. Pieters, …, S. E. Hufton. 2003. Affinity maturation of Fab antibody fragments by fluorescent-activated cell sorting of yeast-displayed libraries. *FEBS Lett.* 546:288–294.
26. Tillotson, B. J., J. M. Lajoie, and E. V. Shusta. 2015. Yeast display-based antibody affinity maturation using detergent-solubilized cell lysates. *In* Yeast Surface Display: Methods, Protocols, and Applications. B. Liu, ed. Springer New York, pp. 65–78.
27. Feldhaus, M. J., R. W. Siegel, …, K. D. Wittrup. 2003. Flow-cytometric isolation of human antibodies from a nonimmune *Saccharomyces cerevisiae* surface display library. *Nat. Biotechnol.* 21:163–170.
28. McMahon, C., A. S. Baier, …, A. C. Kruse. 2018. Yeast surface display platform for rapid discovery of conformationally selective nanobodies. *Nat. Struct. Mol. Biol.* 25:289–296.
29. Bhatia, S. K., J. S. Swers, …, D. A. Hammer. 2003. Rolling adhesion kinematics of yeast engineered to express selectins. *Biotechnol. Prog.* 19:1033–1037.
30. Pepper, L. R., D. A. Hammer, and E. T. Boder. 2006. Rolling adhesion of alphaL I domain mutants decorrelated from binding affinity. *J. Mol. Biol.* 360:37–44.
31. Pepper, L. R., R. Parthasarathy, …, E. T. Boder. 2013. Isolation of αL I domain mutants mediating firm cell adhesion using a novel flow-based sorting method. *Protein Eng. Des. Sel.* 26:515–521.
32. Mann, J. K., D. Demonte, …, S. Park. 2016. Cell labeling and proximity dependent biotinylation with engineered monomeric streptavidin. *Technology (Singap.).* 04:152–158.
33. Dundas, C. M., D. Demonte, and S. Park. 2013. Streptavidin-biotin technology: improvements and innovations in chemical and biological applications. *Appl. Microbiol. Biotechnol.* 97:9343–9353.
34. Laitinen, O. H., H. R. Nordlund, …, M. S. Kulomaa. 2003. Rational design of an active avidin monomer. *J. Biol. Chem.* 278:4010–4014.
35. Wu, S.-C., and S.-L. Wong. 2005. Engineering soluble monomeric streptavidin with reversible biotin binding capability. *J. Biol. Chem.* 280:23225–23231.
36. Qureshi, M. H., J. C. Yeung, …, S. L. Wong. 2001. Development and characterization of a series of soluble tetrameric and monomeric streptavidin muteins with differential biotin binding affinities. *J. Biol. Chem.* 276:46422–46428.
37. Lim, K. H., H. Huang, …, S. Park. 2013. Stable, high-affinity streptavidin monomer for protein labeling and monovalent biotin detection. *Biotechnol. Bioeng.* 110:57–67.
38. Gietz, R. D., and R. A. Woods. 2002. Transformation of yeast by lithium acetate/single-stranded carrier DNA/polyethylene glycol method. *Methods Enzymol.* 350:87–96.
39. Gallant, N. D., and A. J. García. 2007. Quantitative analyses of cell adhesion strength. *Methods Mol. Biol.* 370:83–96.
40. Boettiger, D. 2007. Quantitative measurements of integrin-mediated adhesion to extracellular matrix. *In* Methods in Enzymology: Integrins. D. A. Cheresh, ed. Academic Press, pp. 1–25.
41. Puchner, E. M., G. Franzen, …, H. E. Gaub. 2008. Comparing proteins by their unfolding pattern. *Biophys. J.* 95:426–434.
42. Evans, E., and K. Ritchie. 1997. Dynamic strength of molecular adhesion bonds. *Biophys. J.* 72:1541–1555.
43. Yin, J., P. D. Straight, …, C. T. Walsh. 2005. Genetically encoded short peptide tag for versatile protein labeling by Sfp phosphopantetheinyl transferase. *Proc. Natl. Acad. Sci. USA.* 102:15815–15820.
44. Liu, Z., H. Liu, …, M. A. Nash. 2020. High force catch bond mechanism of bacterial adhesion in the human gut. *Nat. Commun.* 11:4321.
45. Ott, W., M. A. Jobst, …, H. E. Gaub. 2017. Elastin-like polypeptide linkers for single-molecule force spectroscopy. *ACS Nano.* 11:6346–6354.
46. Schwaiger, I., M. Schleicher, …, M. Rief. 2005. The folding pathway of a fast-folding immunoglobulin domain revealed by single-molecule mechanical experiments. *EMBO Rep.* 6:46–51.
47. Brockwell, D. J., G. S. Beddard, …, S. E. Radford. 2005. Mechanically unfolding the small, topologically simple protein L. *Biophys. J.* 89:506–519.
48. Brunk, D. K., and D. A. Hammer. 1997. Quantifying rolling adhesion with a cell-free assay: E-selectin and its carbohydrate ligands. *Biophys. J.* 72:2820–2833.
49. Hammer, D. A. 2014. Adhesive dynamics. *J. Biomech. Eng.* 136:021006.